

Vibronic speed-up of the excitation energy transfer in the Fenna-Matthews-Olson complex

P. Nalbach, C. A. Mujica-Martinez, and M. Thorwart

*I. Institut für Theoretische Physik, Universität Hamburg, Jungiusstraße 9, 20355 Hamburg, Germany
The Hamburg Centre for Ultrafast Imaging, Luruper Chaussee 149, 22761 Hamburg, Germany*

(Dated: January 16, 2022)

We show that the efficient excitation energy transfer in the Fenna-Matthews-Olson molecular aggregate under realistic physiological conditions is fueled by underdamped vibrations of the embedding proteins. For this, we present numerically exact results for the quantum dynamics of the excitons in the presence of nonadiabatic vibrational states in the Fenna-Matthews-Olson aggregate employing an environmental fluctuation spectral function derived from experiments. Assuming the prominent 180 cm^{-1} vibrational mode to be underdamped, we observe, on the one hand, besides vibrational coherent oscillations between different excitation levels of the vibration also prolonged electronic coherent oscillations between the initially excited site and its neighbours. On the other hand, however, the underdamped vibrations provide additional channels for the excitation energy transfer and by this increase the transfer speed by up to 30%.

Recent experiments on the ultrafast exciton dynamics in photoactive biomolecular complexes have sparked renewed interest in the longstanding question whether nontrivial quantum coherence effects exist in natural biological systems under physiological conditions, and, if so, whether they have any functional significance. Photosynthesis [1] starts with the harvest of a photon by a pigment and the formation of a tightly bound electron-hole pair. After the exciton has been formed in the antenna complexes, its energy is transferred to the reaction center (RC), where further charge separation is initiated. The transfer dynamics of the excitations occurs non-radiatively by a Coulomb dipolar coupling and has traditionally been regarded as an incoherent hopping between molecular sites [2].

Recently, Engel et al. [3, 4] have interpreted long-lasting beating signals in time-resolved optical two-dimensional spectra of the Fenna-Matthews-Olson (FMO) complex [5–7] as evidence for quantum coherent energy transfer via delocalized exciton states. The FMO complex is a trimer with seven bacteriochlorophyll (BChl) molecular sites (plus an additional weakly coupled eighth BChl) in each monomer. Quantum coherence times of almost a picosecond at 77 K [3, 4] and about 300 fs at physiological temperatures [4] have been reported.

These reports have boosted on-going research to answer the question how quantum coherence can prevail over such long times in a strongly fluctuating physiological environment formed by the strongly vibrating protein host and the surrounding polarization fluctuations of the ambient water as a strongly polar solvent. Theoretical modeling of the real-time quantum transfer dynamics is difficult due to the non-standard spectral distributions of the fluctuations. In this case, the validity of standard Redfield-type approaches based on a weak-coupling and a Markovian approximation is not clear a priori [8–10]. Simplistic modelling shows that spatial and temporal correlations can in principle allow for prolonged quantum

coherence [11, 12]. A more accurate treatment of the FMO model with seven localized sites and a physical environmental spectrum [13, 14] including a strongly localized Huang-Rhys vibrational mode [2] at thermal equilibrium has been realized. However, the resulting coherence times are considerably shorter than experimentally observed [15]. Very strong underdamped high-frequency vibrations could also be ruled out as a possible origin of the experimentally observed long-lived coherent beatings [16].

Recently, it was proposed that underdamped low frequency vibrations, which are strongly coupled to the electronic transitions with large Huang-Rhys factors, and which are almost resonant to the excitonic transitions, are responsible for the observed long-lived coherence [17–20]. The prominent vibrational mode with a wave number of 180 cm^{-1} was explicitly included in the system’s nonadiabatic quantum dynamics and thus discussed on an equal footing as the excitonic states. By this, Christensson et al. [17] found coherence times in line with experimental findings employing a Redfield approach to treat the environmental fluctuations. Chin et al. [20] observed the same results employing a numerically exact treatment of a partial model which is restricted to an effective FMO model with two of the seven pigments. So far, the full seven site FMO model with the realistic spectrum of its environmental fluctuations is unexplored by numerically exact means. Likewise, the fundamental question how long the quantum coherent beatings survive and how they profit from an interaction with the underdamped low frequency vibration in a realistic setting is open. We aim here at clarifying whether this scenario of excitonic coherence being fueled by vibrational coherence could explain the experiments on an accurate and quantitative level. At the same time possible functional relevance of the underdamped low frequency vibration is not studied so far. We investigate here the influence of the underdamped low frequency vibration on the speed

and thus efficiency of energy transfer through the FMO complex.

In this work, we present numerically exact results for the full FMO model with seven sites, the spectral density of Refs. [13, 14] as extracted from optical spectra [13] and by treating the underdamped vibrational mode with wave number 180cm^{-1} explicitly and at an equal footing as the excitonic quantum dynamics. Upon adopting the iterative real-time quasiadiabatic propagator path-integral (QUAPI) [21–23] scheme we find that the excitonic coherence times are increased by the coherent vibrational modes. We observe not only vibrational coherent oscillations between different excited vibrational states, but also prolonged electronic coherent oscillations between the initially excited site and its neighbours. Most importantly, we show quantitatively that the underdamped vibrational mode provides additional transfer channels for the excitation energy to be funnelled more efficiently through the Fenna-Matthews-Olson molecular aggregate under realistic physiological conditions. We find a substantial speed-up of the transfer times of up to 30%, as compared to the static complex. Although both coherent oscillations and vibronic speed-up originate from the underdamped vibrational mode, the life time of the oscillations is irrelevant for the speed-up resulting in a robust mechanism.

RESULTS

Model of the FMO complex

The FMO monomer contains eight bacteriochlorophyll *a* (BChl*a*) molecular sites [7], of which the recently discovered eighth pigment [24, 25] is only weakly coupled to the other BChls and thus will be omitted in the present investigation. The Hamiltonian restricted to the single excitation subspace for the remaining seven sites is $H_{FMO} = \sum_{j=1}^7 \epsilon_j |j\rangle\langle j| + \sum_{j \neq k} J_{jk} (|j\rangle\langle k| + |k\rangle\langle j|)$, where the basis states $|j\rangle$ indicate that the j -th site is in its excited state and all other sites are in their ground states. ϵ_j denotes the energy of the j -th site and J_{jk} denotes the electronic coupling between sites j and k . We use the numerically determined site energies and dipolar couplings calculated by Adolphs and Renger [14] (the explicit form is given in the Supporting Information). Here, the BChl 3 is the site with the lowest energy which is connected to the RC and forms the exit site [7] out of the FMO complex. BChls 1 and 6 are oriented towards the baseplate protein as indicated by experimental results [7, 26]. These sites are therefore considered as the entrance sites which are the initially excited sites.

The surrounding vibrational pigment-protein-solvent environment induces thermal fluctuations on the excitation transfer dynamics. We treat the electronic states of the FMO complex within an open quantum system

approach [27]. The thermal fluctuations are generated by environmental harmonic modes [2]. Thus the total Hamiltonian is

$$H = H_{FMO} + \sum_{j=1}^7 |j\rangle\langle j| \sum_{\alpha} \kappa_{\alpha}^{(j)} q_{j,\alpha} \quad (1) \\ + \sum_{j=1}^7 \frac{1}{2} \sum_{\alpha} (p_{j,\alpha}^2 + \omega_{j,\alpha}^2 q_{j,\alpha}^2),$$

with momenta $p_{j,\alpha}$, displacements $q_{j,\alpha}$, frequencies $\omega_{j,\alpha}$ and coupling constants $\kappa_{\alpha}^{(j)}$ of the environmental vibrations at site j . We assume that the fluctuations at different BChl sites are identical in their characteristics, but spatially uncorrelated [15]. Within this open quantum system approach, the environmental fluctuations and their coupling to the system dynamics are characterized by their spectral density $G(\omega) = \sum_{j,\alpha} (|\kappa_{\alpha}^{(j)}|^2 / 2\omega_{j,\alpha}) \delta(\omega - \omega_{j,\alpha})$. This distribution function determines the temporal correlations of the environmental fluctuating forces [27]. Here, we use experimentally determined [13] and theoretically parametrized [14] form $G(\omega) = S_0 g_0(\omega) + S_H \delta(\omega - \omega_H)$. This fluctuational spectrum contains both a broad low frequency contribution $S_0 g_0(\omega)$ by the protein vibrations with Huang-Rhys factor S_0 and a single effective vibrational mode of the pigments centered at $\omega_H = 180\text{ cm}^{-1}$ with Huang-Rhys factor $S_H = 0.027$ [13] (the detailed form is given in the SI). Below, we will also study the case of a stronger excitonic-vibrational mode coupling, since Adolphs and Renger have determined a larger Huang-Rhys factor of $S_H = 0.22$ [14]. In general, within the system-bath approach, the environment is commonly assumed to be in a thermal equilibrium state. Thus, including a discrete vibrational mode into the environmental spectrum implicitly assumes that the time scale of thermalization of this mode is much shorter than any system time scale. Then, the discrete mode only provides thermal equilibrium fluctuations around its thermal state. However, recent analyses [17, 20] propose that underdamped vibrational modes are present, which are strongly coupled to the electronic transitions with large Huang-Rhys factors, and which are close to resonance to excitonic transitions. The observed long-lasting coherent signals [3, 4] are then attributed to the coupled exciton - underdamped mode system. In this scenario, the full nonadiabatic quantum dynamics of the vibrational mode has to be considered and not only its thermal equilibrium fluctuations. We therefore include in the following the vibrational mode at 180 cm^{-1} explicitly as part of the *system* Hamiltonian and thus describe its nonequilibrium quantum dynamics on an equal footing as the excitonic states. Due to the exponential growth of needed computer power for QUAPI with increasing system size (see SI), we restrict the localized mode to its three (two) lowest energy eigenstates for site 3 (all others). In detail, we include all states up

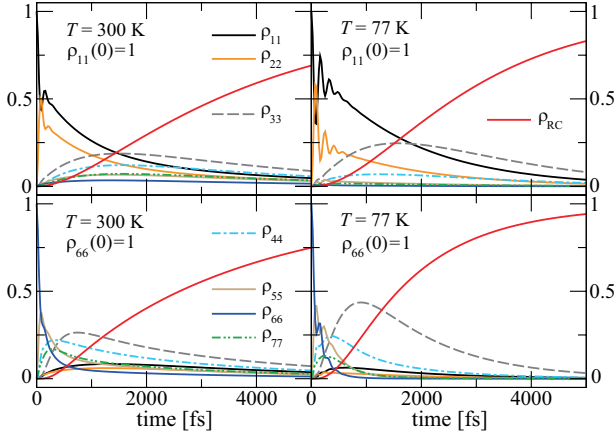


FIG. 1. Time evolution of the FMO site populations and reaction center (RC) in absence of any vibrational mode for $T = 300$ K (left column) and $T = 77$ K (right column) for the initial population of the two entrance sites $\rho_{11}(0) = 1$ (upper row) and $\rho_{66}(0) = 1$ (lower row) for the Huang-Rhys factor $S_H = 0.027$.

to the energy of the site with lowest energy, i.e. site 3, plus two times thermal energy.

Energy transfer dynamics through the FMO complex

In order to discuss the efficiency of the energy transfer through the FMO complex towards the RC, we model the latter as an energy sink which is connected solely to site 3. We treat the transfer towards the RC as a population decay on a purely phenomenological level by constant decay rate of 1 ps^{-1} since we are not interested in the explicit details of the dumping process. Backtransfer from the RC to the FMO complex is then excluded here. In turn, the rise time of the population growth of the RC is taken as a measure for the efficiency of the energy transfer through the complex.

To evaluate the influence of localized vibrational modes on the exciton transfer dynamics, we first provide the excitonic dynamics in absence of any vibrational mode as a reference. Fig. 1 shows the results for the individual site populations along with the population ρ_{RC} of the energy sink. We study two cases of the initial population of the two entrance sites, i.e., $\rho_{11}(0) = 1$ (upper row) and $\rho_{66}(0) = 1$ (lower row) and for the two temperatures $T = 300$ K (left column) and $T = 77$ K (right column). We observe that apart from few oscillations of selected populations at very short times, no long-lasting coherent oscillations in the populations are found. The population of the energy sink increases in a monotonous manner.

Taking the results in Fig. 1 as a reference, we next consider the exciton dynamics when every individual FMO site is coupled to its own vibrational mode. All of them

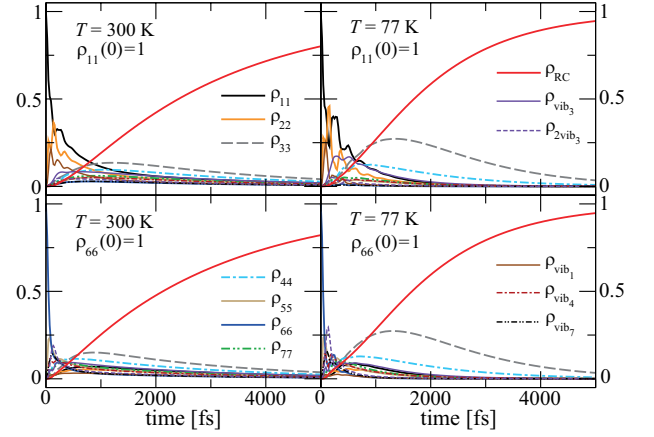


FIG. 2. Same as in Fig. 1 but in presence of individual vibrational modes at each individual molecular site. Vibrational states with energies up to 450 cm^{-1} above the energy of site 3 are included and all vibrational modes have equal characteristics.

are assumed to have equal characteristics and we choose in this section a Huang-Rhys factor of $S_H = 0.027$. The QUAPI method is limited by the exponential growth of the array sizes and the computational times for growing system Hilbert space dimensions (see SI). We thus have to limit the Hilbert space dimensions to vibrational states with energies up to 450 cm^{-1} above the energy of site 3. The exciton eigenstates of the FMO complex, obtained by diagonalizing the FMO system Hamiltonian, show that the included vibrational states have comparable or larger energies. The relevant vibrational modes which influence the system dynamics are those with energies comparable to the energy difference between the exciton states [16]. Thus, the relevant FMO excitonic energy ranges are sufficiently covered, and therefore, the technical restriction of truncated vibrational energies has no severe implications. The results for initially excited entrance sites without vibrational excitation are shown in Fig. 2. We observe both prolonged oscillatory population dynamics with increased coherence times *and* an increased transfer efficiency, as indicated by the faster rise of the population ρ_{RC} of the energy sink.

The increased transfer efficiency can be quantified in terms of the time which is required for the transfer of excitation energy through the FMO complex. A measure for this is the rise time of the exponential growth of the population ρ_{RC} of the RC to which we refer as 'transfer time' in short. The dynamical simulations allow us to read off the rise times, the results are summarized in Table I. We find that, when vibrational modes are coupled to all individual sites separately and including all states with energies up to 450 cm^{-1} above the energy of site 3, the transfer times decreases by about 25%. The speed-up is slightly larger when the initial excitation starts at site 1 due to the shorter route [6]. In the site repre-

TABLE I. Excitation energy transfer times at $T = 300$ K without and with nonequilibrium vibrational modes coupled to the excitonic transitions. A negative change in the transfer time indicates a speed-up, while a positive sign indicates a slower transfer as compared to the case without vibrational states.

Localized vibrational mode coupled to	Initial excitation at site	Transfer time [ps]	Change by
NO vibration	1	3.84	—
	6	3.39	—
all sites (up to 450 cm^{-1})	1	2.86	-25.4 %
	6	2.60	-23.2 %
site 1	1	4.12	+ 7.4 %
	6	3.62	+ 6.9 %
site 3	1	2.62	-31.6 %
	6	2.49	-26.6 %
site 6	1	3.95	+ 2.9 %
	6	3.56	+ 5.0 %

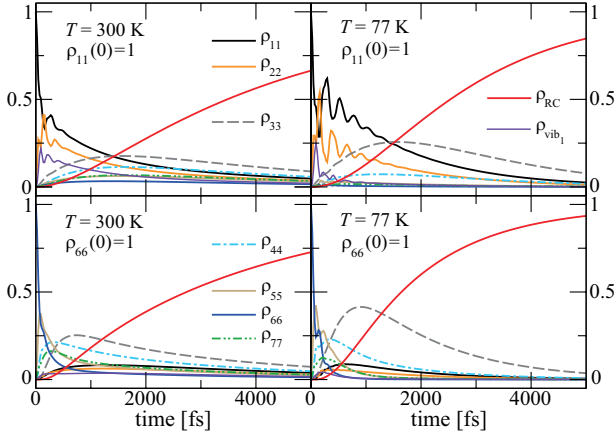


FIG. 3. Time evolution of the populations of the FMO sites, the sink, and the single vibrational mode coupled solely to the entrance site 1.

sensation, this proceeds along the chain $1 \rightarrow 2 \rightarrow 3$. In turn, when the excitation starts at site 6, it follows $6 \rightarrow (5/7) \rightarrow 4 \rightarrow 3$. A speed-up of about 25% is significant.

To further elucidate by which more detailed mechanism the vibrations enhance the coherence times and the transfer efficiency, we study next the excitonic dynamics by including a single localized vibrational mode only at selected sites separately. In particular, we consider the two cases, (i) when the vibrational mode is coupled to the entrance site 1, and (ii) when it is coupled to the exit site 3. The corresponding results are presented in Figs. 3 and 4, respectively. The third case when the vibrational mode is coupled to the other entrance site 6 is discussed in the SI. The resulting energy transfer times at $T = 300$ K for all cases are given in Table I.

When coupling a single vibrational mode to the en-

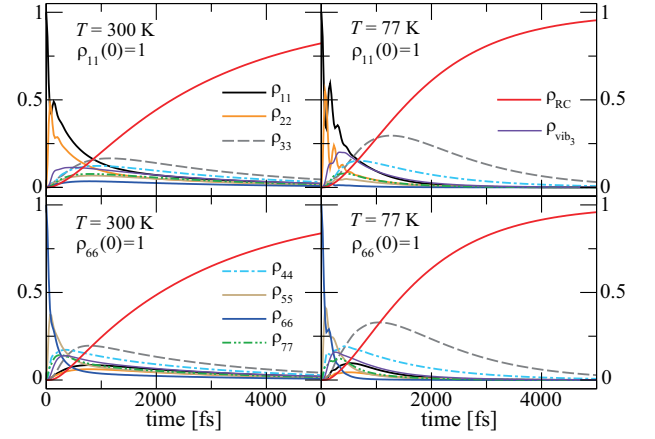


FIG. 4. Same as in Fig. 3, but with the single vibrational mode coupled to the exit site 3.

trance site 1, we observe in Fig. 3 for both values of the temperature, an enlarged time window exists with an oscillatory dynamics of the populations, after which they continue by an incoherent decay. This effect is more pronounced when the site 1 is initially excited (upper row) as compared to an initial preparation in site 6 (lower row). In particular, the energy coherently oscillates between the sites 1 and 2 over several hundreds of femtoseconds. A closer inspection of the dynamics shows that the oscillations in the exciton populations indeed go back to coherent transitions between the vibrational ground state and the vibrational first excited state at site 1. We extract coherence times of about 1000 fs for $T = 77$ K and of 300 fs for $T = 300$ K, which coincide with those reported in the experiments [3, 4]. However, we observe that the associated energy transfer times have *increased* in comparison with the case when vibrational modes are excluded (see Table I). These results prove that the coupling of a nonequilibrium vibrational mode to the entrance site 1 enhances coherence times, but decreases the overall transfer efficiency. The corresponding findings also arise when a single vibrational mode is coupled to the entrance site 6 (see Table I and SI).

On the other hand, when the vibrational mode is coupled to the *exit* site 3, see Fig. 4, the coherence times are not enhanced as compared to the case without any vibrational mode (Fig. 1). This is not surprising since site 3 is only rather weakly coupled to its neighbours and additionally coupled to the RC acting as an incoherent energy sink. However, it is important to realize that the population of the sink grows faster in this constellation and, consequently, the transfer efficiency is increased, as seen in Table I. This speed-up of the transfer efficiency is a key observation and can be directly rationalized in terms of an additional transfer channel which is provided by the excited vibrational state at site 3. This excited vibrational state is nearly in resonance with the electronic transition and thus decreases the energy gap with the

entrance sites. By this, it adds an additional efficient pathway in form of a vibrational decay channel into the RC. Accordingly, more states connected to the RC are available to become populated during the exciton transfer in the complex and, consequently, more states can dump their energy into the sink in parallel. The population of the sink then can grow faster and yields to an overall increased transfer efficiency.

Overall, the underdamped modes at 180 cm^{-1} improve the efficiency of the quantum coherent excitation energy transfer and at the same time result in the observed prolonged quantum coherent oscillations. Both are a result of the modes being underdamped, such that they cannot thermalize on time scales fast compared to the electronic energy transfer dynamics. Beyond that, the speed-up of the energy transfer is rather insensitive to the actual coherence life times.

Population dynamics in the FMO complex

Having studied the effect of nonequilibrium vibrational states on the exciton transfer efficiency, we study next the impact of a larger coupling of the vibrational mode and the electronic transitions, i.e., for a larger Huang-Rhys factor. So far, we have considered an intermediate exciton-vibrational coupling. Based on the data of the temperature dependence of the fluorescence line-narrowing spectra, Wendling et al. [13] have determined a Huang-Rhys factor $S_H = 0.027$. This corresponds to a coupling strength of 30 cm^{-1} (see the SI for details). On the other hand, Adolphs and Renger [14] have found a Huang-Rhys factor of $S_H = 0.22$ for the vibrational mode at 180 cm^{-1} , which is about one order of magnitude larger. This corresponds to a vibrational coupling strength of 84 cm^{-1} . These two values correspond to the regime of the intermediate and the strong exciton-vibrational mode coupling, respectively. We show next that for the strong coupling regime, the same physical picture applies as in the intermediate regime considered so far, but small quantitative differences arise (see Table S1 in the SI).

Here, we focus on the study of the transient coherent oscillations and do not include the additional sink at the exit site 3. The results in Figs. 5 and 6 show the cases when the vibrational mode is coupled to the entrance site 1 and to the exit site 3, respectively. The case when the vibrational mode is coupled to the second entrance site 6 is discussed in the SI. A single initial condition $\rho_{11}(0) = 1$ is chosen for both cases at physiological ($T = 300\text{ K}$) and cryogenic ($T = 77\text{ K}$) temperatures.

When the underdamped vibrational mode is strongly coupled to the initially excited site 1, we observe in Fig. 5 (lower row) on the one hand strong beatings in the populations between the vibrational ground state and the vibrational first excited state at site 1. On the other hand,

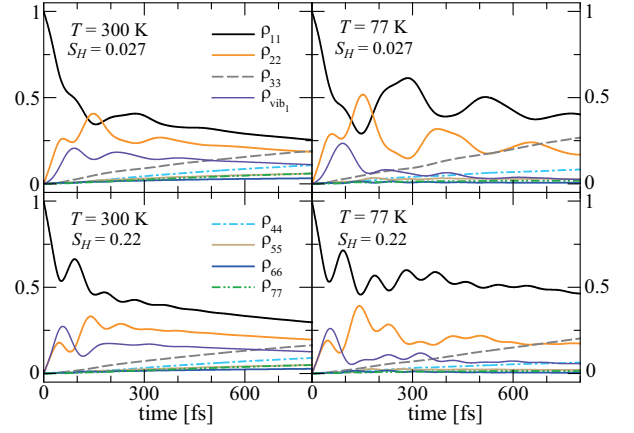


FIG. 5. Time evolution of populations of the FMO sites and the first excited state of the vibrational mode coupled to the entrance site 1 in absence of the reaction center. We show the results for the initial condition $\rho_{11}(0) = 1$ for $T = 300\text{ K}$ (left column) and $T = 77\text{ K}$ (right column) for an intermediate ($S_H = 0.027$, upper row) and a strong ($S_H = 0.22$, lower row) exciton-vibrational mode coupling.

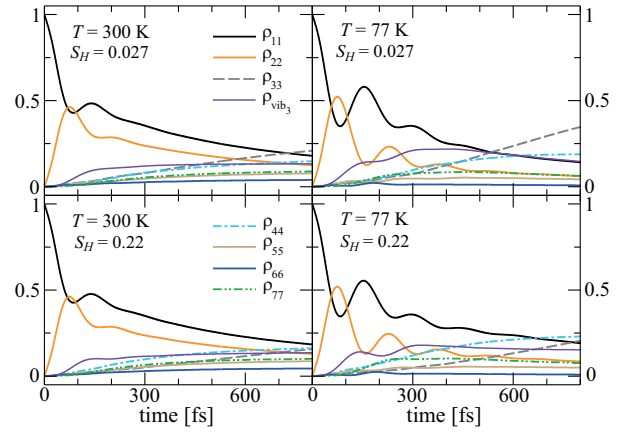


FIG. 6. Same as in Fig. 5, but with the vibrational mode coupled to the exit site 3.

however, we also find coherent beatings between exciton sites 1 and 2 without excitation of the vibrational state. At room temperature, coherent oscillations survive for up to about 400 fs and at 77 K for at least up to 800 fs. These coherence times are comparable to those of the experiments [3, 4]. For an intermediate value of the exciton-vibrational coupling, we observe in Fig. 5 (upper row) longer intersite coherence times of around 1000 fs. In this case, the excitonic coupling between sites 1 and 2 is relatively larger than the vibrational coupling of the vibrational ground and first excited states at site 1. On the other hand, in the strong coupling regime longer intrasite coherence times are obtained because the coupling of the vibrational ground at site 1 is of the same order of magnitude as the coupling to the site 2 or to its vibrational excited state. This competition is reflected by

the faster rise of the population of the vibrational first excited state at site 1.

When coupling the vibrational mode to the exit site 3 but initially exciting site 1, we see in Fig. 6 that the coherence times are comparable with those observed without explicitly taking an underdamped 180 cm^{-1} mode into account, see Ref. [15]. This is a result of the fact that the two sites 1 and 3 are only very weakly coupled. At room temperature, coherence survives for up to about 250 fs and at 77 K for up to 600 fs at most in both regimes of the coupling. Nevertheless, we observe a fast increase in the population of the vibrational first excited site 3 $\rho_{\text{vib}_3}(t)$ which is even faster than the population accumulation in its vibrational ground state $\rho_{33}(t)$. This fast population accumulation is a result of the refined matching of the energies of site 1 and of site 3 when exciting the vibrational state while tunneling. This is another remarkable finding, since site 3 is believed to be the exit site towards the reaction center and a larger population of site 3 will result in an overall increased transfer efficiency through the FMO complex towards the reaction center, irrespective of the excitation status of the vibration. Thus, underdamped vibrational modes indeed improve the overall energy transfer efficiency.

These results show that an additional underdamped vibrational mode at site 3 increases the transfer efficiency since it provides additional channels for the parallel decay of the energy into the RC. In contrast, additional underdamped vibrational states at other sites (see SI) tend to decrease the transfer efficiency since they provide additional states in which the energy is intermittently stored and eventually dissipated via the vibrational channel or fed back into the excitonic network at a later stage. Hence, only an efficiently connected exit site helps to improve the global transfer, while additional states at the intermediate sites only lead to an inefficient spreading-out of the energy into too many channels.

DISCUSSION

We have obtained numerically exact results for the real-time nonequilibrium quantum dynamics of the excitation energy transfer through the FMO complex in presence of realistic environmental fluctuations and an underdamped localized vibrational mode at 180 cm^{-1} . Our analysis shows that the coupling of the excitonic transitions to a nearly resonant vibrational mode causes strong vibrational quantum coherent beatings in the intrasite populations of individual pigments. At the same time, however, the nearly resonant coupling also causes strong coherent excitonic beatings in the intersite population transfer between different pigments. However, prolonged coherent intersite beatings do not necessarily lead to an enhanced transfer efficiency. We show that only the additional vibrational states at the exit site 3

of the FMO complex help to speed-up the global energy transfer by providing additional transfer channels to the exit site towards the reaction center. In fact, they lead to a speed-up of up to 30% in the transfer times through the complex. Long-lasting coherence in the complex results from the coupling of the vibrational modes to particular entrance and exit sites. It is, however, not functionally necessary for the enormous speed-up of energy transfer which thus is a rather robust mechanism.

These results offer a benchmark principle which may be implemented in artificial light-harvesting systems as well. Their global quantum transfer efficiency can be significantly increased by engineering the corresponding almost resonant vibrational modes, thereby maintaining the number of absorbing photoactive sites constant.

We acknowledge financial support by the DFG Sonderforschungsbereich 925 "Light-induced dynamics and control of correlated quantum systems", by the German Academic Exchange Service (DAAD) and by the excellence cluster 'The Hamburg Centre for Ultrafast Imaging - Structure, Dynamics and Control of Matter at the Atomic Scale' of the Deutsche Forschungsgemeinschaft.

-
- [1] van Amerongen H, Valkunas L, van Grondelle R (2000) *Photosynthetic Excitons* (Singapore, World Scientific).
 - [2] May V, Kühn O (2011) *Charge and Energy Transfer Dynamics in Molecular Systems* (Weinheim, Wiley-VCH), 3rd Ed.
 - [3] Engel GS, et al. (2007) Evidence for wavelike energy transfer through quantum coherence in photosynthetic systems. *Nature* 446: 782-786.
 - [4] Panitchayangkoon G, et al. (2010) Long-lived quantum coherence in photosynthetic complexes at physiological temperature. *Proc Natl Acad Sci USA* 107: 12766-12770.
 - [5] Matthews B, Fenna R, Bolognesi M, Schmid M, Olson J (1979) Structure of a bacteriochlorophyll *a*-protein from the green photosynthetic bacterium *Prosthecochloris aestuarii*. *J Mol Biol* 131: 259-285.
 - [6] Brixner T, et al. (2005) Two-dimensional spectroscopy of electronic couplings in photosynthesis. *Nature* 434: 625-628.
 - [7] Milder MTW, Brüggemann B, van Grondelle R, Herek JL (2010) Revisiting the optical properties of the FMO protein. *Photosynth Res* 104: 257-274.
 - [8] Ishizaki A, Fleming GR (2009) On the adequacy of the redfield equation and related approaches to the study of quantum dynamics in electronic energy transfer. *J Chem Phys* 130: 234110.
 - [9] Nalbach P, Thorwart M (2010) Multiphonon transitions in the biomolecular energy transfer dynamics. *J Chem Phys* 132: 194111.
 - [10] Nalbach P, Ishizaki A, Fleming GR, Thorwart M (2011) Iterative path-integral algorithm versus cumulant time-nonlocal master equation approach for dissipative biomolecular exciton transport. *New J Phys* 13: 063040.
 - [11] Thorwart M, Eckel J, Reina JH, Nalbach P, Weiss S (2009) Enhanced quantum entanglement in the non-

- markovian dynamics of biomolecular excitons. *Chem Phys Lett* 478: 234-237.
- [12] Nalbach P, Eckel J, Thorwart M (2010) Quantum coherent biomolecular energy transfer with spatially correlated fluctuations. *New J Phys* 12: 065043.
 - [13] Wendling M, et al. (2000) Electron-vibrational coupling in the Fenna-Matthews-Olson complex of *Prosthecochloris aestuarii* determined by temperature-dependent absorption and fluorescence line-narrowing measurements. *J Phys Chem B* 104: 5825-5831.
 - [14] Adolphs J, Renger T (2006) How proteins trigger excitation energy transfer in the FMO complex of green sulfur bacteria. *Biophys J* 91: 2778-2797.
 - [15] Nalbach P, Braun D, Thorwart M (2011) Exciton transfer dynamics and quantumness of energy transfer in the Fenna-Matthews-Olson complex. *Phys Rev E* 84: 041926.
 - [16] Nalbach P, Thorwart M (2012) The role of discrete molecular modes in the coherent exciton dynamics in FMO. *J Phys B: At Mol Opt Phys* 45: 154009.
 - [17] Christensson N, Kauffmann HF, Pullerits T, Mančal T (2012) Origin of long-lived coherences in light-harvesting complexes. *J Phys Chem B* 116: 7449-7454.
 - [18] Mančal T, et al. (2012) System-dependent signatures of electronic and vibrational coherences in electronic two-dimensional spectra. *J Phys Chem Lett* 3: 1497-1502.
 - [19] Tiwari V, Peters WK, Jonas DM (2013) Electronic resonance with anticorrelated pigment vibrations drives photosynthetic energy transfer outside the adiabatic framework. *Proc Natl Acad Sci USA* 110: 1203-1208.
 - [20] Chin AW, et al. (2013) The role of non-equilibrium vibrational structures in electronic coherence and recoherence in pigment-protein complexes. *Nat Phys* 9: 113-118.
 - [21] Makri N, Makarov DE (1995) Tensor propagator for iterative quantum time evolution of reduced density matrices. I. Theory. *J Chem Phys* 102: 4600-4610.
 - [22] Thorwart M, Reimann P, Jung P, Fox R (1998) Quantum hysteresis and resonant tunneling in bistable systems. *Chem Phys* 235: 61-80.
 - [23] Nalbach P, Thorwart M (2009) Landau-Zener transitions in a dissipative environment: Numerically exact results. *Phys Rev Lett* 103: 220401.
 - [24] Tronrud DE, Wen J, Gay L, Blankenship RE (2009) The structural basis for the difference in absorbance spectra for the FMO antenna protein from various green sulfur bacteria. *Photosynth Res* 100: 79-87.
 - [25] Schmidt am Busch M, Müh F, El-Amine Madjet M, Renger T (2011) The eighth bacteriochlorophyll completes the excitation energy funnel in the FMO protein. *J Phys Chem Lett* 2: 93-98.
 - [26] Wen J, Zhang H, Gross ML, Blankenship RE (2009) Membrane orientation of the FMO antenna protein from *Chlorobaculum tepidum* as determined by mass spectrometry-based footprinting. *Proc Natl Acad Sci USA* 106: 6134-6139.
 - [27] Weiss U (2008) *Quantum Dissipative Systems* (Singapore, World Scientific), 3rd Ed.